The momentum spectra of nuclear active particles in the cosmic radiation at sea level. I. Experimental data

1974 J. Phys. A: Math. Nucl. Gen. 7 741

(http://iopscience.iop.org/0301-0015/7/6/010)

J. Phys. A: Math., Nucl. Gen., Vol. 7, No. 6, 1974. Printed in Great Britain.

The momentum spectra of nuclear active particles in the cosmic radiation at sea level I. Experimental data

I S Diggory, J R Hook†, I A Jenkins‡ and K E Turver
Department of Physics, University of Durham, South Road, Durham City, UK

Received 5 October 1973, in final form 21 November 1973

Abstract. A cosmic ray spectrograph has been used to measure the momentum spectra of cosmic ray protons and pions in the momentum range 1–30 GeV/c in the near vertical direction at sea level. The observed intensities of both protons and pions are greater than those obtained in the previous measurements.

1. Introduction

The momentum spectrum of cosmic ray protons at sea level in the momentum range 1–30 GeV/c is of interest because it may lead to useful comment on the primary spectrum at energies up to 10^4 GeV. The spectrum of pions is of similar interest but probes the primary energy spectrum to higher energies and reflects the characteristics of high energy interactions at energies beyond those available from accelerators.

Measurements of spectra of nuclear active particles at momenta in excess of 0·7 GeV/c have been made by Brooke *et al* (1964), using a magnet spectrograph and neutron monitor. In such an experiment the deflections of single particles are measured in the magnetic field and those particles which are nuclear active are identified by the evaporation neutrons they produce in a neutron monitor. This paper describes equipment similar in principle to that used by Brooke and Wolfendale (1964) and comprises a large air gap magnet spectrograph and a neutron monitor. The equipment of the present experiment is considerably larger, provides more detailed information on the particles but does not have as high a momentum resolution as the earlier device. A comparison of the data reported here with the results of computer simulations for the propagation of particles through the atmosphere is made in a further paper (Hook and Turver 1974, to be referred to as II).

We describe in § 2 the equipment and its constituent parts together with the results of the many checks made to ensure their correct operation; § 3 contains a description of the procedure involved in reducing the data to a form suitable for the analysis which in turn is described in § 7. In § 4 we present data on neutron production in lead by protons in the momentum range 1–30 GeV/c, a topic of some considerable interest and necessary information for an understanding of the response of neutron monitors. The corrections made to the basic data are described in § 5 and the method adopted to derive the absolute fluxes of protons and pions is described in § 6.

†Now at the National Coal Board, Doncaster.
‡ Now at the Department of Civil Engineering, University of Newcastle upon Tyne.

2. The equipment

2.1. General features

The equipment is located at Durham (latitude 54·5 °N, longitude 1·3 °W and an altitude of 65 m) and the measurements were made during January–February 1971 in a period of 986·8 hours. During this time the effective on-time, due allowance being made for the dead time of the instrument, was $1{\cdot}56 \times 10^6$ s; the number of single particles in the cosmic ray beam selected using the apparatus was 867 617 of which 10 273 were accompanied by a response in the neutron monitor and were recorded by the equipment.

2.2. The magnet spectrograph

2.2.1. The air gap magnet. The magnet had a useful volume of 0·1 m^3 with a maximum magnetic flux density of 0·45 T when a current of 30 A was passed through the coils dissipating up to 12 kW of power, which was removed by forced air cooling. The magnet current, which was recorded continuously, showed a variation of less than $\pm 3\%$; these variations have been ignored.

The design of the magnet was unusual and was developed to incorporate materials available from the solid iron 'picture frame' type magnets, used by O'Connor and Wolfendale (1960) and Earnshaw *et al* (1967). Pairs of iron plates from a 'picture frame' magnet were placed side by side and cut to the shape indicated in figure 1. Twenty four of these pairs of plates were then placed on top of each other and firmly bolted together, to form the main body of the magnet with a thickness of 30 cm. Coils of copper wire (C, D) were wound around the poles and, to increase the magnetic flux density in the air gap, further coils (A, B) were wound around the main body of the magnet.

The magnetic flux density at each of a matrix of points in and around the air gap of the magnet was measured with a calibrated Hall effect probe. The results are shown in figure 2, from which it can be seen that the flux density was uniform over a large proportion of the air gap and that the variations over the useful region of the air gap were negligible. The magnetic field within the flash tube arrays A3 and B3, which are marked

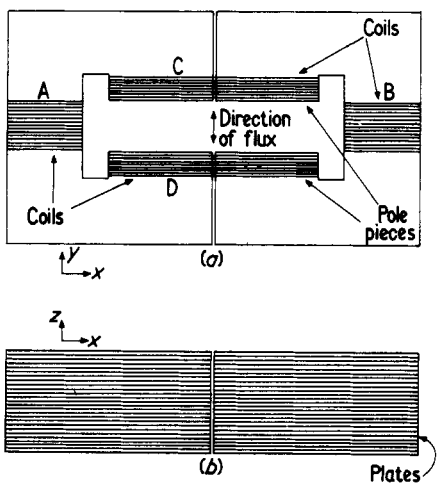

Figure 1. The magnet; (*a*) plan, (*b*) end elevation.

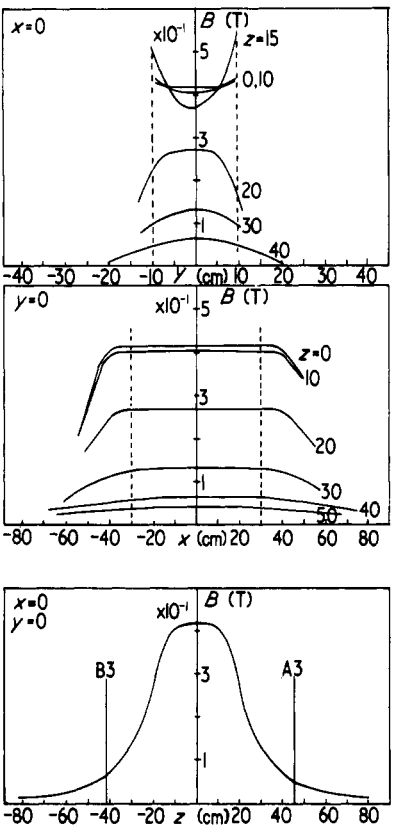

Figure 2. The magnetic flux density in the useful region of the magnet. The broken lines indicate the limits of acceptance for particles defined by the Geiger–Müller counters.

on figure 3, was measured; the line integral of the field shows that the deflection of particles within these trays was negligible. These measurements gave a value for the path length integral, $\int B\,dl$, of 250 kG cm for an energizing current of 30 A.

2.2.2. The flash-tube detectors. Neon flash tubes, developed by Conversi and Gozzini (1955) and Gardener *et al* (1957) have been used successfully in large spectrographs (Hayman and Wolfendale 1962, Earnshaw *et al* 1967) and formed the large area visual detectors in the present experiment. The flash tubes were of mean internal diameter 1·6 cm, mean external diameter 1·8 cm and filled with neon gas to a pressure of 60 cm Hg. The size and disposition of the flash-tube trays and the magnet are shown in figure 3. The detectors A1, A3, B3 and B1 (the momentum trays) provide four estimates of the track location of the momentum determination. The trays A1 and B1 contain 10 layers of 94 tubes, each of length 120 cm, whilst trays A3 and B3 contain 10 layers of 76 tubes (each of length 60 cm), and define the areas through which the particle must enter and leave the magnet to be in the region of uniform induction. The vertical pitch of the flash-tube layers within each tray was 3·2 cm and the centres of the tubes in a layer were separated by $1{\cdot}907 \pm 0{\cdot}008$ cm, giving a maximum layer efficiency of 84%. The tubes in each layer were supported at their ends in slots accurately machined in rectangular duralumin tubing and their positions relative to the magnet were known to $\pm 0{\cdot}2$ mm.

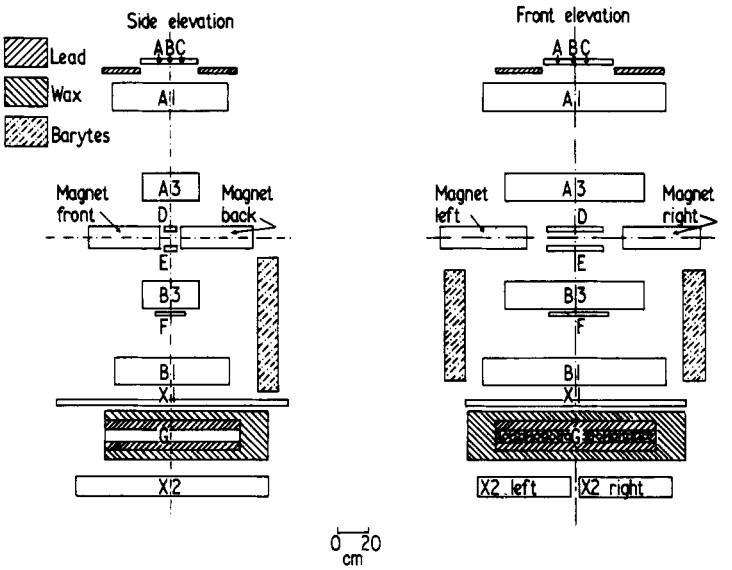

Figure 3. The spectrograph. A, B, C, D, E, F Geiger–Müller counters; A1, A3, B3, B1 10 layers 17 mm diameter tubes; X1 4 layers 17 mm diameter tubes; X2 12 layers 17 mm diameter tubes; G BF_3 counters.

A tray containing four layers of close packed neon flash tubes of length 2·5 m (tray X1, figure 3) was placed immediately above the neutron monitor. This flash-tube tray (the 'neutron monitor shield') indicated the presence of charged particles incident on the neutron monitor, but which, not having passed through the spectrograph, may lead to incorrect identification of particles. The charged particles emerging from the neutron monitor were observed using two trays of neon flash tubes (the 'sub-monitor trays') situated beneath the neutron monitor (X2, figure 3). Each tray consisted of 642 neon flash tubes of length 200 cm deployed in 12 close-packed layers. These trays were used to measure the lateral position of a particle emerging from the neutron monitor, which, when compared with the expected position, due allowance being made for the scattering of a muon in the material of the neutron monitor, enabled the particles to be identified. The accuracy of location of the flash tubes of tray X2 corresponded to a precision of 1 mm in the estimation of the lateral position (a muon of momentum 3 GeV/c would be scattered in the material of the monitor by 10 mm). The trays were positioned side by side and the effect of the gap between the tubes of the two trays on the acceptance function and particle identification was allowed for in subsequent analysis.

The high voltage pulses applied to the flash-tube trays were generated by discharging a capacitor through a thyratron and the primary winding of a high voltage pulse transformer, the technique used in the early applications of flash tubes. The flash tubes were operated in the multiple pulsed mode described by Brooke *et al* (1964) in which the tubes have a memory which retains the information on those flash tubes which have discharged for a period of milliseconds. This storing of flashed tube information enabled the selection requirements involving the (delayed) detection of neutrons in the neutron monitor to be completed. Details of the flashed tubes could then be recorded photographically after fulfilment of the selection requirement and the opening of the camera shutters.

The layer efficiency of the momentum measurement trays was measured to be 69 % for protons, which typically are minimum ionizing, when operated in the multiple pulsed mode. When allowance was made for the geometry of the trays, this corresponded to an internal efficiency of 82 %. This value was lower than expected from a consideration of the geometry alone since there were additional losses of efficiency due to the finite time delay before the application of the initial pulse in the flash tubes (some 6 μs), the non-unit probability of after-flashing (the memory of the tube is not 100 %), and the reduction of the effective aperture of the recording cameras by the shutters. An estimate of the latter two factors was made by measuring the efficiency for cosmic ray beam muons and operating with the shutters permanently open and again with them removed. The first of these measurements removed the loss of efficiency due to the probability of after-flashing while the second allowed an estimate to be made of the effect of the shutters. The probability of after-flashing was found to be 0·95 per pulse while a reduction in layer efficiency of 5 % resulted from the presence of the shutters. The true internal efficiency of the flash tube was therefore at least 91 %.

The particle tracks in the spectrograph were recorded on 35 mm HP4 film using two cameras. The camera shutters used were of the venetian blind type located in front of the cameras and opened in 13 ms.

2.2.3. The neutron monitor. The design of the standard neutron monitor adopted for studies of the low-energy nucleon component of cosmic rays during the International Geophysical Year (IGY) was developed by Simpson (1957) and a detailed discussion of neutron monitors, particularly their response to low-energy nucleons (energy less than 1 GeV) has been given by Hatton (1971).

In the present experiment an improved response was required to increase the efficiency of detection of nuclear interacting particles and so a modified neutron monitor was used. (It is important to note that the neutron monitor used in the earlier experiment of Brooke and Wolfendale (1964) which has been referred to as a 'standard IGY monitor' was not so; the device had in fact an effective neutron detection efficiency some 50 % higher than the standard instrument.) The average thickness of the lead target for particles incident from the vertical was increased in the present device from 13·5 cm to 23·3 cm (264 g cm^{-2} or 1·32 interaction lengths). According to the calculations of Shen (1968), this should result in an increase in the number of neutrons produced. It would be expected that the mean multiplicity of the detected neutrons would be increased relative to the standard IGY neutron monitor, because of this increased value of the number of neutrons produced. However the thicker lead increased the number of negative muons which were captured by the lead nuclei and the number of neutrons produced in interactions of muons by a factor of two, compared with 40 % for the increased number of interactions from the other components. The mean multiplicity of the evaporation neutrons produced in both these muon processes is small (about two for negative muon capture and nine for muon interactions) and will not be increased by a thicker lead producer layer. The increased contribution from these low multiplicity processes will tend to reduce the mean multiplicity of detected neutrons and a consideration of the expected performance of the present neutrons and monitor leads to a predicted mean multiplicity of 1·2. The mean multiplicity recorded by the monitor, having the greatest similarity, the Leeds IGY neutron monitor, was found to be 1·24 (Hatton 1971) for a detection efficiency of 3 %. This would reduce to a value of 1·2 for a detection efficiency of 2 %, a value more appropriate to the present monitor which has a gating efficiency of 67 %. Thus it is expected that although the rate of neutrons detected should

be increased the mean recorded multiplicity of the neutrons would not change much with respect to the earlier Leeds IGY monitor; enhancement of the high-energy response of the modified neutron monitor will only become apparent when the multiplicity distribution from interactions of high-energy charged particles is considered.

The overall efficiency for the detection of thermal neutrons was increased by increasing the number, the size and gas pressure of the neutron detectors used in the standard monitor. Ten cylindrical proportional counters (20th Century Electronics, type 107 EB70/50G) of diameter 5 cm and sensitive length 1·07 m filled with ^{10}B-enriched BF_3 gas at a pressure of 70 cm Hg were used. It should be noted that the anticipated increase in efficiency due to the increased diameter and gas pressure of the counters will be offset to some extent by the larger volume accessible to the evaporation neutrons due to the thicker producing layer. This reduces the density of the evaporation neutrons and so the overall efficiency with which they are detected. The signals from each proportional counter were recorded separately to provide information on the region of production of the neutrons in an attempt to improve the identification of the particles. The shaped pulses from each BF_3 counter were fed to ratemeters and the counting rate of each of the counters was continuously monitored.

Tests were carried out to measure the characteristics of the neutron monitor to confirm that it was operating satisfactorily and to obtain an understanding of its response.

The dependence of the total counting rate on atmospheric pressure. The attenuation, or barometric, coefficient of the counting rate of the monitor, β, as defined by

$$dN = -\beta N\, dP$$

where N is the counting rate and P is the atmospheric pressure, was found to be 1·08 % (mm Hg)$^{-1}$ at 760 mm Hg, in reasonable agreement with the precise value of

$$(0{\cdot}991 \pm 0{\cdot}007)\,\%\,(\text{mm Hg})^{-1}$$

found by Griffiths *et al* (1966) for the Leeds IGY monitor.

The distributions in the arrival time of recorded neutrons. The arrival time distributions were measured by displaying the shaped pulses from the counters on an oscilloscope and photographing the trace. Zero time was defined as the time of the interaction which produced the evaporation neutrons, and this was taken as the time of detection of the charged particle which interacted in the monitor. Figure 4 shows the measured time distribution for this neutron monitor compared with the equivalent distribution for the Leeds IGY neutron monitor (Hatton and Tomlinson 1968). The time distributions are in good agreement over the range of times measured (40–340 μs) and follow an exponential law.

The distributions in the recorded multiplicities. The multiplicity distribution for each BF_3 counter was measured using a neutron-multiplicity recorder triggered by a detected neutron. This gave the multiplicity distribution and the overall counting rate for each counter and so the uniformity of the response across the monitor. The counting rate of each of the counters in the monitor, as shown in figure 5, indicated that counters 4 and 6 were counting the neutrons produced by the low-energy background radiation at a lower rate than the other counters. There was no detectable difference between the multiplicity distributions of the counters; the mean multiplicity of a single counter was 1·08. The effect on the counting rate of the monitor of the material of the spectrograph

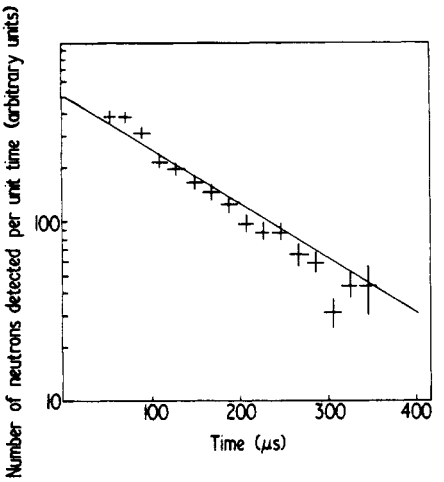

Figure 4. The distribution in real time of the neutrons observed in the modified neutron monitor (full line: Hatton and Tomlinson 1968).

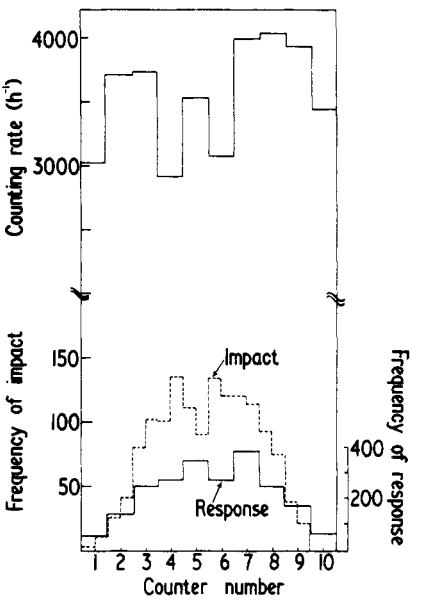

Figure 5. The counting rate of individual counters in the monitor (upper full line); the point of impact of particle tracks on the monitor (lower broken line) and the neutron counters which detected the neutrons produced by nuclear interacting particle events (lower full line) are also shown.

located above was measured to be a decrease of 50% in the overall counting rate determined in the absence of the shielding.

As a further check on the uniformity of the monitor the events used in the measurement of the momentum spectra of protons and pions were analysed to give distributions of: (i) the point of impact of the particle tracks on the neutron monitor, and (ii) the

proportional counters which detected the neutrons in the recorded nuclear interacting particle events.

These distributions are shown in figure 5 and in neither does the apparent inefficiency of counters 4 and 6 appear. Since these distributions were derived from data used in the measurements of the momentum spectra, it is concluded that the monitor was responding uniformly to the (relatively) energetic particles which are of interest in the measurement.

A detailed report on the neutron monitor, including details of the determination of its efficiency will be given later.

2.2.4. Single particle selection system. Charged particles passing through the spectrograph were detected by four trays of Geiger–Müller counters (20th Century Electronics, type G60 of length 60 cm and diameter 3 cm). Three trays each containing 10 tubes (ABC in figure 3) were located on top of the spectrograph. Two trays (DE in figure 3) each containing 11 counters arranged in two close-packed layers were located in the air gap of the magnet and a tray of 10 counters (F in figure 3) was installed underneath the neon flash tube tray B3. The shaped pulses from the three sets of detectors were fed into coincidence units and throughout the study of single nuclear interacting particles to be described the following combination was used:

$$(A+B+C).(D.E).F.$$

No provision was made for the electronic rejection of the events with more than one particle incident upon the spectrograph. As a check on the operation of the Geiger-counter trays, the rates of pulses from each of the units were monitored on a ratemeter. Events meeting the above requirements and accompanied by neutron monitor response were selected and a paralysis of 2·1 s applied immediately after triggering the whole system. If a neutron was detected within the sensitive time of the neutron gate (40–340 μs) the sequence of events indicated in figure 6 was initiated. The multiplicity of

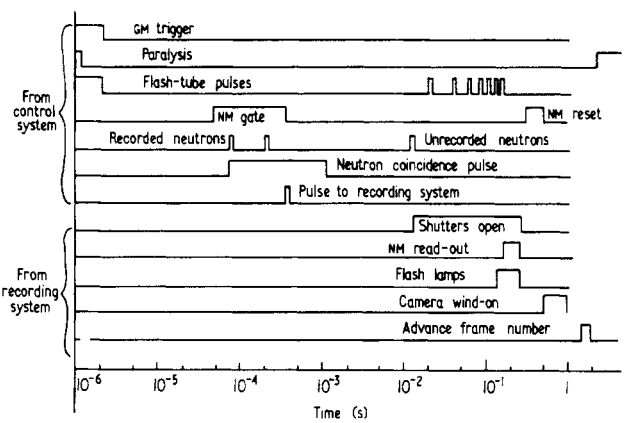

Figure 6. The sequence of events during the recording of a particle.

neutrons detected in each counter was recorded by each camera and the detection time of the neutrons was recorded by direct photography of an oscilloscope trace using a third camera.

3. The analysis of the spectrograph data

3.1. General

The following data were available for each event recorded by the spectrograph: (*a*) the tracks of particles in the spectrograph; (*b*) the magnitude and polarity of the magnetic field; (*c*) the multiplicity of the neutrons detected in each proportional counter in the neutron monitor and their detection time relative to the time of arrival of the interacting particle, and (*d*) the tracks of any particles which emerged from the neutron monitor.

This information must be retrieved from the film records and converted to a form which can be analysed conveniently to provide spectra of the angular deflection of hadrons in the magnetic field, from which their momentum spectrum may be derived.

The deflection of a particle is measured by reconstructing its track through the spectrograph to give its arrival direction projected on the measurement plane of the spectrograph and its angle of emergence from the region of the magnetic field. Having thus determined the angular deflection, a knowledge of the actual position of the particle track in the neutron monitor, the region of detection of the neutrons, and the scattering of any secondaries emerging from the neutron monitor led to the identification of the particle. Deflection spectra for positive and negatively charged nuclear interacting particles may thus be obtained. It is assumed that there are no antiprotons in the cosmic radiation near sea level, and that the momentum spectra of positive and negative pions are identical, when the momentum spectrum of protons and pions may be derived.

3.2. The track reconstruction

3.2.1. The outline method. Methods previously used for track reconstruction involve the adjustment of a cursor over a scale model of the flash-tube array (Hayman and Wolfendale 1962) or the use of a computer technique (Bull *et al* 1962). The former method suffers from the disadvantages of being slow, subjective and limited in accuracy by the precision with which the scale model is constructed and so a computer method was devised for the present experiment.

Most methods of computer analysis of tracks have utilized a probability $P(z)$ that a tube will flash when a particle traverses it at a distance z from its centre. A likely trajectory was set up and the probability of the observed pattern of flash tubes in the flash-tube trays occurring was calculated. Various possible trajectories were then considered and that trajectory which gave the highest probability was regarded as the best estimate of the actual trajectory of the particle. It was found that using this procedure the best estimate track was sensitive to the form of the probability function which was not necessarily well known. In view of these disadvantages a computer track-fitting method was devised to give the best simulation of the well proved hand-analysis method which maximizes the track length in flashed tubes traversed and minimizes the track length in the non-flashed tubes traversed.

Having estimated the best track for each arm of the spectrograph independently, various parameters, some of which indicate the acceptability of the best track and others which are needed for the later derivation of the momentum spectra, are calculated. These include:

(*a*) the angular deflection of the particle;

(*b*) the approximate impact point of the best track on the neutron monitor; for the purposes of this measurement the neutron monitor was split up at the level of the top

of the inner wax moderator into 80 cells and the cell in which the best track impacted was calculated;

(*c*) the momentum corresponding to the deflection in the magnetic field (no allowance being made for Coulomb scattering or errors in track location); and

(*d*) the apparent electric charge of the particle.

On completion of the analysis of the track in the spectrograph any track in tray X2 was analysed to sufficient accuracy in a least-squares fit to the flashed tubes, leading to estimates of the coordinates of the centre of gravity of the flashed tubes and the angle of inclination of the track to the vertical.

3.2.2. Tests on the validity of the procedure for track fitting. The reliability of the track-fitting program was checked in the following ways.

(i) Computer fitting was compared with the results of the analyses made using a large simulator for 200 events. Scale drawings ($\frac{2}{3}$ actual size) of each half of the spectrograph were constructed and used to give estimates of the trajectory of the particle (the hand-analysis method). Figure 7 shows a plot of the best fit from the computer analysis against the best fit from the hand analysis; inset is a histogram of the difference in those values. It can be seen that there is good agreement between the trajectories given by the computer program and those from the hand analysis; it is concluded that if the hand analysis gives a good estimate of the trajectory then so will the present computer analysis.

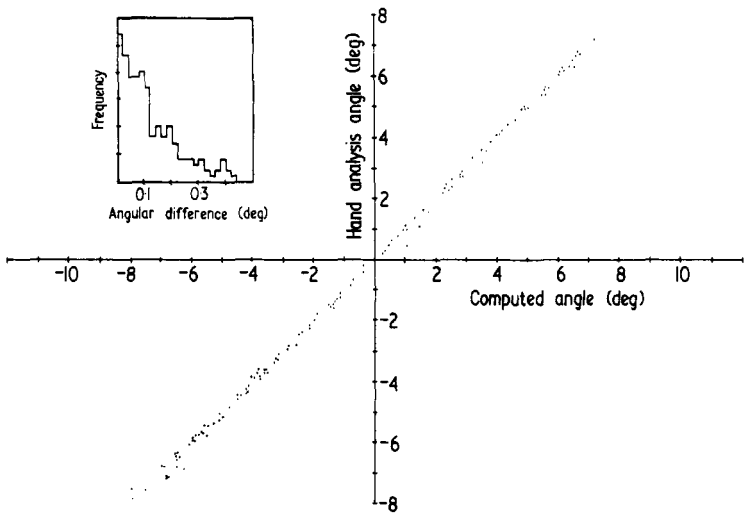

Figure 7. A comparison of the track fitting procedures. The distribution in angular differences between hand analysis and computer analysis is shown inset.

(ii) Artificial tracks with known angles and lateral positions were generated by Monte Carlo methods and the results of fitting by the computer program were compared with the known parameters. The artificial events were generated by selecting a trajectory randomly in the two trays of flash tubes in an arm of the spectrograph and then determining through which flash tubes a trajectory passed. For each tube the probability of flashing was then determined using a probability function, and it was then decided by Monte Carlo methods whether the tube had flashed. The events generated in this

way were analysed using the computer program and the resulting best track compared with the known trajectory. It has been shown that the precise form of the probability function used in generating the tracks is not important and three different forms of function were considered. In each case the RMS angular difference between the actual artificial track and the best track selected by the computer was less than 0·1°.

(iii) The momentum spectrum of cosmic ray muons was measured and analysed using the track-fitting program and compared with the previous measurements of the spectrum. About 1000 events were recorded by the spectrograph when triggered solely by a counter coincidence (A + B + C) . (D . E) . F which were predominantly unassociated muons and they were analysed in the same way as the single particles constituting the nuclear interacting particle spectrum. The value of apparent momentum was determined for each event and the resulting integral spectrum is shown in figure 8, where it is compared with the spectrum of Allkofer *et al* (1971). The two spectra are arbitrarily normalized at a momentum of 1 GeV/c and *no* corrections for scattering and instrumental errors have been applied to the present spectrum; the agreement is good up to a momentum of about 20 GeV/c, indicating that the present analysis techniques may be reliably used up to this value *without any corrections*, and to higher momenta if appropriate allowance is made for scattering effects.

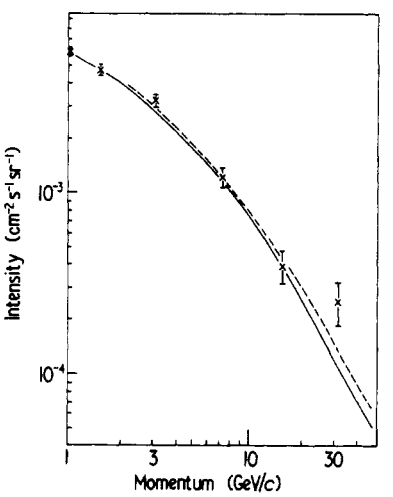

Figure 8. The integral momentum spectrum of muons. Full curve: Hayman and Wolfendale (1962); broken curve: Allkofer *et al* (1971). The experimental parts are obtained from the present instrument in the absence of any corrections whatsoever.

3.2.3. The estimation of the measurement noise in track location. When a vertical particle of momentum p passes through the spectrograph it is deflected through an angle $\Delta\psi_m$ by the magnetic field, where

$$\Delta\psi_m = \frac{K}{p}.$$

However, on traversing the material of the spectrograph the particle is scattered by collision with nuclei and when the track is reconstructed a random error is made in

estimating the angle of the best fit, assumed to be normally distributed about the actual trajectory. In general the actual measured deflection $\Delta\psi$ will not equal $\Delta\psi_m$ but a beam of vertical particles of momentum p will give a distribution of measured deflections such that

$$p(\Delta\psi)\,d\Delta\psi = \frac{1}{\sigma\sqrt{2\pi}} \exp\left(\frac{-(\Delta\psi - \Delta\psi_m)^2}{2\sigma^2}\right) d\Delta\psi$$

where $p(\Delta\psi)\,d\Delta\psi$ is the probability of observing a deflection $\Delta\psi$ to $\Delta\psi + d\Delta\psi$. The standard deviation, σ, of this distribution is given by

$$\sigma^2 = \sigma_c^2 + \sigma_T^2$$

σ_c is the RMS value of scattering due to collision with nuclei, given by $\sigma_c = 0{\cdot}148\sqrt{x/p\beta}$ where x is the thickness of the material traversed in radiation lengths, β is the velocity of the particle in terms of velocity of light and σ_T is the RMS value of the error due to track reconstruction and is a constant.

In order to reduce σ_T to a low value, the neon flash tubes were accurately located and σ_T was estimated to be between 0·1° and 0·2°. For the purpose of the analysis to be described later, the value of σ_T of $0{\cdot}15 \pm 0{\cdot}03°$ has been assumed, and the small effects of the uncertainty in σ_T at the momenta considered here have been fully considered.

3.3. The impact criteria for trajectories in the neutron monitor

The evaporation neutrons emitted by an excited nucleus are characterized by isotropic angular distribution and an energy spectrum which is peaked around a few MeV (Hatton 1971). The cross section for elastic scattering of 2 MeV neutrons is about 1 b and the angular scattering distribution is peaked in the forward direction. Under the assumption that neutrons are detected by the counter in the moderator on which they are incident, the majority of evaporation neutrons will be detected in the nearest counter since this counter subtends the largest solid angle at the excited nucleus. It is therefore expected that the majority of the evaporation neutrons will be detected close to the point of production.

The neutron monitor was divided into 80 cells of approximate width 2 cm and the cell upon which the best track was calculated and the number of cells from this point to the nearest counter which had detected a neutron was estimated as the impact distance. Figure 9 shows the distribution of impact distances obtained for all the analysed events and superimposed on this distribution is the distribution which will be expected if all the events were muons in accidental coincidence with a neutron monitor response which was uniform across the neutron monitor, being typical of background counts. These distributions indicate that the evaporation neutrons are indeed detected close to their production point and these data will aid the identification of particles.

Figure 10 shows the distribution of impact distances for events which can be directly identified by their absorption in the produced layer of the monitor as nuclear interacting particles. The expected distribution of impact distances, calculated on the above assumptions, is drawn on the same figures and the similarity of the distributions indicates that the assumptions are not unreasonable. From these results an impact distance of less than 15 cells was considered necessary for particles to be identified as genuine nuclear interacting particle events.

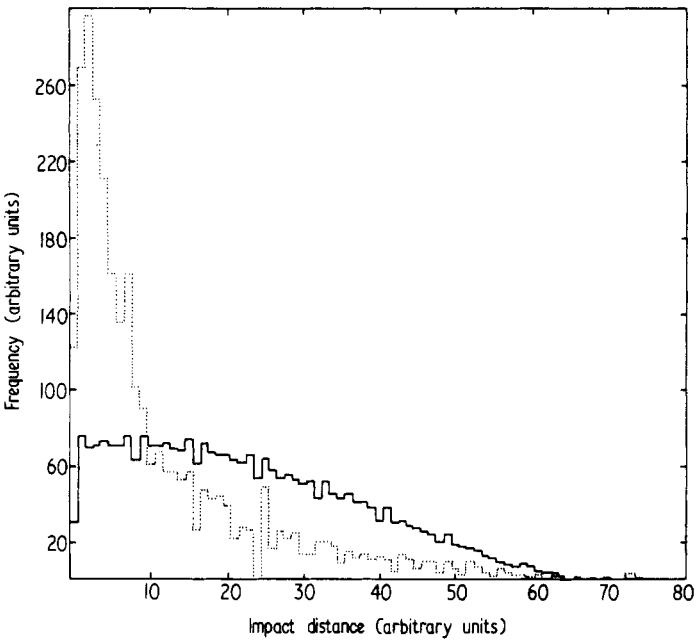

Figure 9. The frequency distribution of the distance between point of impact of a particle on the monitor and the portion of the recorded neutrons. The broken line is the observation and the full line represents the distribution expected if all the particles were muons.

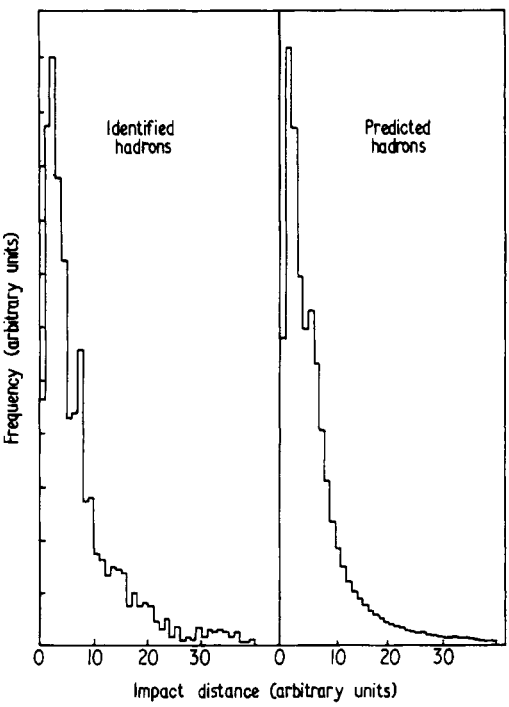

Figure 10. The distribution in impact distance for events identified by their absorption in the monitor as being nuclear active.

3.4. The identification of particles

The following analysis is based on that developed by Brooke and Wolfendale (1964) and assumes that there are no antiprotons in the cosmic radiation at sea level, an assumption which will be discussed further later. With this assumption, there are four categories of single particle which may be expected to be recorded by the present equipment: (i) nuclear active particles consisting of protons and positive and negative pions; (ii) low-energy negative muons which stop in the neutron monitor and are captured by lead nuclei; (iii) muons which have produced neutrons by photonuclear interaction, and (iv) cosmic ray particles, predominantly muons, in accidental coincidence with a neutron derived from the low-energy background recorded by the neutron monitor.

Each event may be placed accurately into one of these four categories using the data available from the film record and track analysis which included the deflection of the particles in the magnetic field which leads to estimates of the momentum and charge, the impact point on the neutron monitor of the particle, the location and time detection of the neutrons recorded in the neutron monitor and the number and location of any particles emerging from the neutron monitor.

The momentum of muons which will just penetrate the monitor of thickness 264 g cm^{-2}, is 0·45 GeV/c according to Joseph (1969). Events of measured momentum less than 1 GeV/c are rejected and the frequency of low-energy negative muons, which will not penetrate the monitor, will be much reduced. Similarly, any particle which has a measured momentum greater than 1 GeV/c together with a monitor response and is absorbed in the neutron monitor may be readily identified as a nuclear interacting particle.

The nuclear interacting particles were selected and their distribution in the measured deflections of positive and negative particles was compiled.

4. The number of neutrons produced by protons in lead

A knowledge of the number of neutrons produced in the lead of the neutron monitor by protons of known momentum is a necessity for the accurate understanding of the response of the monitor.

Assuming that the neutron production is represented by a single exponential, following Cocconi *et al* (1950),

$$I(\nu) = (\mathrm{e}^{a} - 1)\,\mathrm{e}^{-a\nu},$$

where

$$\sum_{0}^{\infty} I(\nu) = 1$$

and

$$\nu = (1 - \mathrm{e}^{-a})^{-1},$$

the mean observed number of neutrons is given by

$$\bar{m} = \nu(\epsilon f) + 1$$

where (ϵf) is the product of the gating efficiency and the detection efficiency for neutrons, allowing for excitation of a nucleus with emission of ν evaporation neutrons when $\nu = 0, 1, 2, \ldots$.

The observational data are shown in figure 11 and the values for ν derived therefrom would probably be an underestimate by 5–10% because of the assumption of a single exponential production spectrum. Discussion of these data and a comparison with the prediction of Shen (1968) will be given elsewhere.

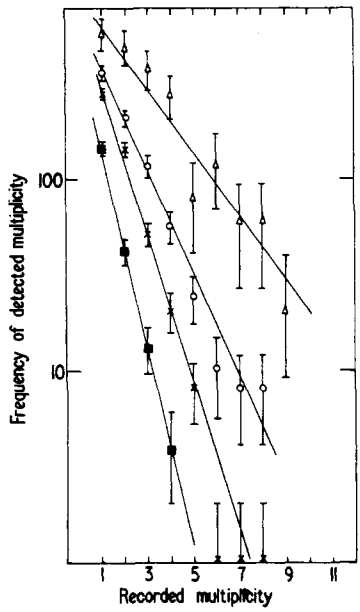

Figure 11. The distribution in multiplicity of recorded neutrons for positive hadrons (predominantly protons) of various momenta. ⊥, 1–1·5 GeV/c; ⊥, 1·5–3 GeV/c; ○, 3–7·5 GeV/c; △, 7·5–15 GeV/c.

5. The corrections to the distribution of angular deflections

Corrections were applied to the basic data to allow for the following errors.

(*a*) The losses due to the incorrect identification of nuclear interacting particles as muons caused by the limit applied to the scattering criterion;

(*b*) the loss of genuine nuclear interacting particles in which the track in the lower half of the spectrograph would have passed between the two trays of flash tubes beneath the neutron monitor;

(*c*) the loss of genuine nuclear interacting particles which had an impact distance greater than the arbitrary limit applied;

(*d*) the identification of slow negative muons appearing to have a momentum of greater than 1 GeV/c resulting from scattering in the material of the spectrograph, in coincidence with a recorded (accidental) neutron;

(*e*) the loss of events through the rejection of tracks having 3 or fewer tubes in a momentum measurement flash tube tray, which would not provide a reliable track reconstruction.

Figure 12 gives the final deflection distributions for positive and negative particles after application of the above corrections.

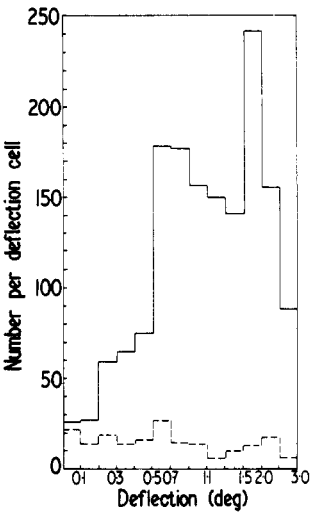

Figure 12. The angular deflection distributions for positive (full histogram) and negative (broken histogram) nuclear active particles.

6. The determination of absolute particle fluxes

The analysis of the corrected data for angular deflections to be described in § 7 yields the shapes of the momentum spectra of protons and negative pions at ground level together with their relative intensities, but does not give their absolute intensities. To obtain the absolute intensities the acceptance of the spectrograph must be evaluated accurately and this is a difficult task since Geiger–Müller counters were used to define the sensitive areas and the effective size of each counter must be accurately measured. An alternative procedure is to normalize the spectra for protons and pions and muons derived in the present experiment to the absolute intensity of the muon spectrum available from other measurements. In the measurement of the muon spectrum in the present experiment the number of events with a measured momentum greater than 1 GeV/c was recorded together with the on-time of the equipment. These data together with the values for intensity of muons of momentum greater than 1 GeV/c given by Allkofer *et al* (1971) indicate a value for the acceptance of the spectrograph of 52 cm^2 sr. The intensities quoted from the present experiment are based on this figure and a sensitive time of $1{\cdot}56 \times 10^6$ s. During this period there occurred 867 617 trigger signals (predominantly muons) of which 10 273 were accompanied by a response from the neutron monitor. These latter events which satisfied the electronic election criteria may be classified after full analysis, as shown in table 1.

7. The derivation of the momentum spectra

7.1. General

The information concerning momentum of nuclear active particles (NAP) is contained in two distributions of angular deflection in the magnetic field, one for positive NAP and one for negative NAP. The nuclear active particles which might reasonably be

Table 1. The types of events which fulfill the triggering requirement of the instrument and their relative frequency.

Type	(%)
Dense events	15
EAS events having more than 1 analysable track	< 1
Events with momentum less than 1 GeV/c	22
NAP of momentum greater than 1 GeV/c	22
Rejected events	6
Muons of momentum greater than 1 GeV/c	15
Interactions in flash-tube trays	19

considered to exist in cosmic rays near sea level are nucleons, antinucleons, pions and kaons. The relative yield of kaons to pions in proton–proton collisions at 70 GeV is 0·1 according to Antipov *et al* (1971) and the kaon lifetime is approximately half that of the pion; the number of kaons in cosmic rays at sea level may therefore be assumed to be negligible compared with the number of pions. The yield of antiprotons in p–p collisions at 70 GeV is 2% of that of negative pions according to Antipov *et al*, although recent evidence indicates that this yield increases with energy (Albrow *et al* 1972). The number of antiprotons should therefore, be small and since there is no evidence to date for their existence in the cosmic radiation at sea level, it is here assumed that the particles detected are exclusively protons and positive and negative pions. It is also assumed that the spectra of positive and negative pions are identical at these angles, and with these assumptions it is possible to derive the momentum spectra of protons and negative pions in the cosmic radiation at ground level, following the procedures described in appendix 1.

7.2. The derivation of the momentum spectra for protons and pions

The momentum spectra are derived from the distribution in angular deflection using the method described by Orford (1968) in which an arbitrary momentum spectrum is taken as a starting point. This spectrum is converted to a spectrum of angular deflection appropriate to our instrument using the appropriate combination of weighting factors (which are described in appendix 2). The spectrum is then modified using a comparison between the predicted and observed deflection spectra such that

$$S_{J+1}(p)\,\mathrm{d}p = \frac{\Sigma_i[S_j(p)W(p,\Delta\psi_i)M(\Delta\psi_i)/N_j(\Delta\psi_i)]\,\mathrm{d}p}{\Sigma_i W(p,\Delta\psi_i)}$$

where $W(p,\Delta\psi_i)$ is the appropriate combined weighting factor, $M(\Delta\psi_i)$ is the deflection spectrum predicted from $S_j(p)\,\mathrm{d}p$ given by $\int S_j(p)W(p,\Delta\psi_i)\,\mathrm{d}p$ and is normalized to $M(\Delta\psi_i)$.

This process is repeated until the value of χ^2 found when comparing the predicted and observed distributions in deflection changes by less than 1% between two successive iterations. A typical best fit deflection distribution compared with the observational data is shown in figure 13.

7.3. The corrections to the spectral shapes

The method of deriving the spectral shapes described above leads to a set of values of

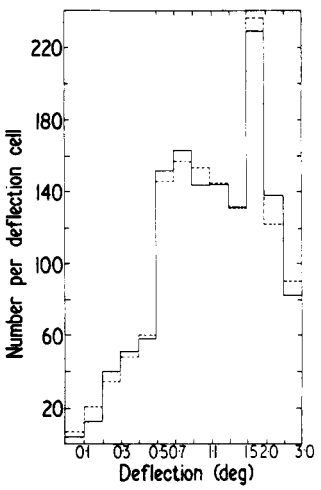

Figure 13. The spectrum of angular deflections in the magnetic field of the spectrograph for protons (full histogram: observed; broken histogram: predicted).

the intensity at a particular momentum but there are momentum-dependent corrections which remain to be applied to the spectrum, as follows.

(i) The loss of particles due to interaction in the spectrograph. The probability of particles traversing the spectrograph without undergoing either electromagnetic or nuclear interaction was calculated as a function of momentum and particle type, and is shown in figure 14.

(ii) The loss of particles due to the low efficiency of the neutron monitor. If the multiplicity spectrum of evaporation neutrons produced in an interaction of a given energy can be represented by a single exponential law, then the probability of not detecting any neutrons is given by $1/\bar{m}$, where $\bar{m}$ is the average number of detected neutrons. Values for this quantity for various proton momenta are given in § 4. The

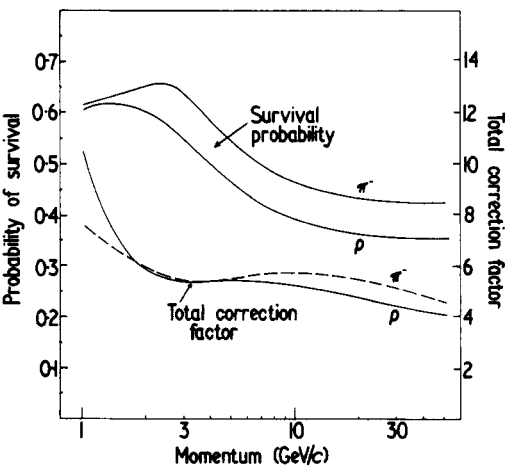

Figure 14. The probability of survival of protons and pions in traversing the material of the spectrograph. The lower curves represent the total correction factors to be applied to the measured spectrum (see text for details).

correction to be applied to the spectral shape is $\bar{m}/(\bar{m}-1)$ and is a function of momentum but is independent of the value of efficiency of the neutron monitor, which for the purposes of the present experiment, need not be known.

(iii) The loss of particles due to the transparency of the neutron monitor. A particle must undergo at least one nuclear interaction in the lead target of the monitor if it is to be detected and the probability of such interactions is a function of momentum. The interaction probability was estimated for a target of thickness 268 g cm^{-2} using the variation of the total interaction cross section given by Giacomelli (1970). These three correction factors were combined to give the total correction factor as a function of momentum, shown in figure 11, and applied to momentum spectra derived as described in § 7.2.

The differential momentum spectra so obtained were then integrated and statistical errors added to each point on the integral spectrum. (The small errors in momentum arising from the uncertainty on the estimated value of the error in angular measurement have been neglected.) The steepest and flattest acceptable integral spectra were drawn through the extremities of the statistical error bars and each of the spectra was differentiated numerically to give the upper and lower limits appropriate to the differential intensities.

7.4. The momentum spectrum of unaccompanied protons near sea level

Figure 14 shows the distribution of deflections of protons measured in the present experiment and has been obtained by subtracting the distribution of negative NAP, as described in appendix 1. The predicted deflection distribution obtained from the best-fit momentum spectrum found using the technique described above is also shown in the figure. The best-fit momentum spectrum is shown in figure 15 where it is compared with the data of Brooke and Wolfendale (1964) and the differential intensities are tabulated in table 2. It should be noted that the previous measurements were normalized

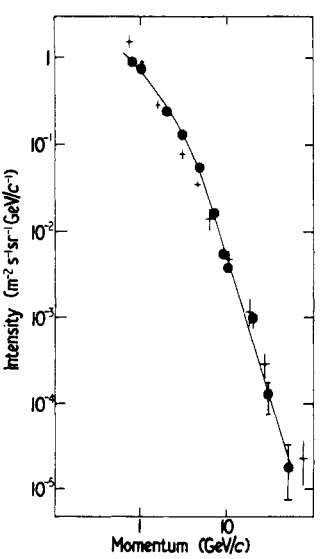

Figure 15. The differential momentum spectrum of single, unaccompanied protons at sea level (+, Brooke and Wolfendale 1964; ⧫, present work).

Table 2. The differential intensities of single protons at sea level.

Proton momentum (GeV/c)	Intensity ($m^{-2}s^{-1}sr^{-1}(GeV/c)^{-1}$)
1	$(7{\cdot}45^{+0{\cdot}10}_{-0{\cdot}18}) \times 10^{-1}$
2	$(2{\cdot}37^{+0{\cdot}5}_{-0{\cdot}3}) \times 10^{-1}$
3	$(1{\cdot}22^{+0{\cdot}2}_{-0{\cdot}3}) \times 10^{-1}$
5	$(5{\cdot}31 \pm 0{\cdot}18) \times 10^{-2}$
7	$(1{\cdot}66 \pm 0{\cdot}09) \times 10^{-2}$
10	$(3{\cdot}76 \pm 0{\cdot}3) \times 10^{-3}$
20	$(9{\cdot}27^{+0{\cdot}78}_{-1{\cdot}31}) \times 10^{-4}$

to the intensity of 1 GeV/c muons obtained by Rossi (1948), whereas the present data are normalized to the intensity given by Allkofer *et al* (1971) which is about 20% greater. The experimental points of Brooke and Wolfendale should therefore be increased by 20% if the more recent absolute intensity experiment is to be preferred. There is reasonable agreement between the results from the two measurements bearing in mind the large corrections made to the basic data (see figure 14). However, the present work produces a somewhat different spectral shape from the simple power law which can be fitted to the earlier data; such a curved spectrum may be expected to arise from the ionization loss of the protons in the atmosphere. Furthermore between 2 and 10 GeV/c, there is some suggestion in the present data for an increased flux of protons.

7.5. Momentum spectrum of unaccompanied negative pions near sea level

The data of the best fit momentum spectrum are given in table 3 and are presented in figure 16, where they are compared with the data of Brooke *et al* (1964) from which the negative pion intensities were obtained by halving the published charged pion intensities. Again, the absolute intensities of Brooke *et al* and the present work were obtained by normalization to the absolute muon intensities quoted by Rossi (1948) and Allkofer *et al* (1971), respectively. The shapes of the two spectra are similar but the intensities obtained from the present work are systematically higher by a factor of up to two than those of Brooke *et al*; part of this discrepancy may be attributed to the different normalization procedures used to obtain absolute fluxes, but there still remains a discrepancy of more than 1·5 at all momenta.

Table 3. The differential intensities of single negative pions at sea level.

Pion momentum (GeV/c)	Intensity ($m^{-2}s^{-1}sr^{-1}(GeV/c)^{-1}$)
1	$(5{\cdot}68 \pm 0{\cdot}25) \times 10^{-2}$
2	$(2{\cdot}08 \pm 0{\cdot}08) \times 10^{-2}$
3	$(8{\cdot}60 \pm 0{\cdot}39) \times 10^{-3}$
5	$(6{\cdot}48 \pm 0{\cdot}46) \times 10^{-3}$
7	$(4{\cdot}02 \pm 0{\cdot}37) \times 10^{-3}$
10	$(1{\cdot}67 \pm 0{\cdot}21) \times 10^{-3}$
20	$(8{\cdot}53 \pm 1{\cdot}30) \times 10^{-4}$

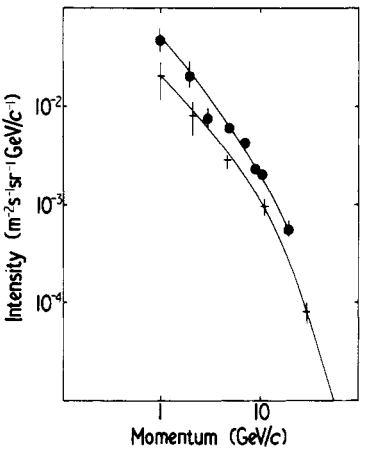

Figure 16. The differential momentum spectrum of single, unaccompanied negative pions at sea level (+, Brooke *et al* 1964; ●, present work).

8. Discussion and conclusions

The data from the present experiment may only be usefully compared with results from one other experiment—that of Brooke and Wolfendale (1964). It appears from figures 15 and 16 that although overall the spectra appear in reasonable agreement, there is some indication of an excess of particles of momentum 2–10 GeV/c in the present data. This is clearly so for the spectrum of negative pions shown in figure 16 which is found in the present experiment to be consistently of higher intensity than was found in the earlier work.

Extensive investigations of the present and earlier measurements based both on published material and unpublished material made available by Wolfendale (1972, private communication) have given no indication of the reasons for the difference.

To remove dependences upon analysis and normalization procedures the data are perhaps best expressed in the form of the $\pi^{\pm}$/p ratio and this is shown in figure 17. It is seen that at momenta in the range 2–10 GeV/c the data for this ratio from the two experiments are in reasonable agreement; the measurement at a momentum of 10 GeV/c in the earlier experiment is in agreement with the present data although the fit ascribed by the previous authors to their data was significantly below this point. The implication of the good agreement in $\pi^{\pm}$/p ratio, and hence spectral shape, in the momentum range 2–10 GeV/c is that the difference in the experiments may lie in the values used for the correction factors shown in figure 14. We have no data, however, which confirm this or any other possibility. The difference in the spectra at higher momenta would be expected in measurements on single unaccompanied particles made using two different instruments. The differences arise from the variations in the spectra of hadrons measured in detectors of different size; our larger instrument has a greater probability of detecting an accompanying particle than had the earlier equipment, and so is less sensitive to those (energetic) hadrons produced by energetic primaries. This loss in sensitivity causes a steepening of the spectra and a deviation from the shape of the primary spectrum; it is most important in the momentum range 10–100 GeV/c for the protons.

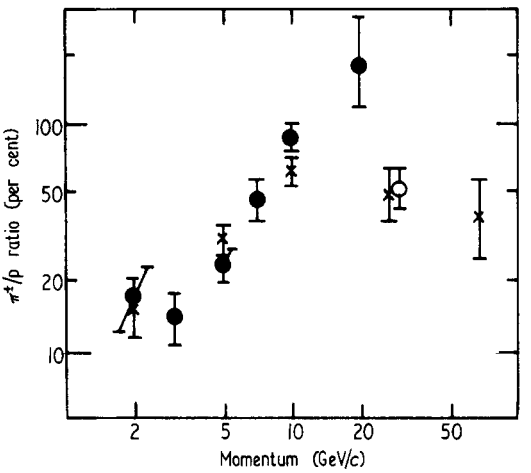

Figure 17. The ratio of single pions (+ and −) to protons at sea level (⊻, Brooke *et al* 1964; ●, present work; ○, Subrahmanian 1962).

The agreement between the previous (sea level) measurement and the measurement made at an atmospheric depth of 800 g cm^{-2} by Subrahmanian (1962) is perhaps fortuitous since it appears that no allowance for the effect of the differences in atmospheric depth of the observation level has been made. It seems likely that on the basis of measurements for the ratio of charged to neutral particles of energy greater than or of the order of 100 GeV made at various depths between 600 and 800 g cm^{-2} the $\pi^{\pm}/p$ ratio may be expected to be higher at sea level than at 800 g cm^{-2}.

We conclude therefore that the bulk of the data from the two magnetic spectrograph experiments and that from the measurements of Subrahmanian are compatible with a ratio of the intensities of single pions to single protons at sea level which increases from a value of 10% at 1 GeV to about 100% at 10–20 GeV.

An interpretation of these data on the basis of model calculations for the propagation of cosmic rays through the atmosphere and measurement using a detector as described here will be given in a later paper by Hook and Turver (1974).

Acknowledgments

The authors are grateful to Professor G D Rochester FRS and Professor A W Wolfendale, for their continued support and helpful suggestions during this measurement.

The contributions in the early stages of the experiment by Drs K J Orford, J C Earnshaw, B D O'Donnell, and Messrs A B Walton and G C Maslin are gratefully acknowledged.

The Science Research Council are thanked for financial support.

Appendix 1. Separation of spectra of protons and pions

Let $K_p S_p(p)\,dp$, $K_{\pi^+} S_{\pi^+}(p)\,dp$, $K_{\pi^-} S_{\pi^-}(p)\,dp$ be the momentum spectra of protons, positive pions and negative pions respectively. Then the observed deflection spectra for

positive particles, $N_+(\Delta\psi)\,\mathrm{d}\Delta\psi$, and negative particles $N_-(\Delta\psi)\,\mathrm{d}\Delta\psi$ will be

$$N_+(\Delta\psi)\,\mathrm{d}\Delta\psi = \int_0^\infty K_p S_p(p) W_p(p,\Delta\psi)\,\mathrm{d}p\,\mathrm{d}\Delta\psi + \int_0^\infty K_{\pi^+} S_{\pi^+}(p) W_{\pi^+}(p,\Delta\psi)\,\mathrm{d}p\,\mathrm{d}\Delta\psi + \int_0^\infty K_{\pi^-} S_{\pi^-}(p) \overline{W}_{\pi^-}(p,\Delta\psi)\,\mathrm{d}p\,\mathrm{d}\Delta\psi$$

and

$$N_-(\Delta\psi)\,\mathrm{d}\Delta\psi = \int_0^\infty K_p S_p(p) \overline{W}_p(p,\Delta\psi)\,\mathrm{d}p\,\mathrm{d}\Delta\psi + \int_0^\infty K_{\pi^+} S_{\pi^+}(p) \overline{W}_{\pi^+}(p,\Delta\psi)\,\mathrm{d}p\,\mathrm{d}\Delta\psi + \int_0^\infty K_{\pi^-} S_{\pi^-}(p) W_{\pi^-}(p,\Delta\psi)\,\mathrm{d}p\,\mathrm{d}\Delta\psi,$$

where $W_k(p,\Delta\psi)$ and $\overline{W}_k(p,\Delta\psi)$ are the probabilities of a particle of type k, of momentum p, giving a measured deflection $\Delta\psi$ with the correct and incorrect charge, respectively. But we assume $K_{\pi^+} = K_{\pi^-} = K_\pi$ and $S_{\pi^+}(p)\,\mathrm{d}p = S_{\pi^-}(p)\,\mathrm{d}p = S_\pi(p)\,\mathrm{d}p$ for all p. Then

$$N_+(\Delta\psi)\,\mathrm{d}\Delta\psi = \int_0^\infty K_p S_p(p) W_p(p,\Delta\psi)\,\mathrm{d}p\,\mathrm{d}\Delta\psi + \int_0^\infty K_\pi S_\pi(p)[W_\pi(p,\Delta\psi) + \overline{W}_\pi(p,\Delta\psi)]\,\mathrm{d}p\,\mathrm{d}\Delta\psi$$

and

$$N_-(\Delta\psi)\,\mathrm{d}\Delta\psi = \int_0^\infty K_p S_p(p) \overline{W}_p(p,\Delta\psi)\,\mathrm{d}p\,\mathrm{d}\Delta\psi + \int_0^\infty K_\pi S_\pi(p)[W_\pi(p,\Delta\psi) + \overline{W}_\pi(p,\Delta\psi)]\,\mathrm{d}p\,\mathrm{d}\Delta\psi.$$

Subtracting

$$[N_+(\Delta\psi) - N_-(\Delta\psi)]\,\mathrm{d}\Delta\psi = \int_0^\infty K_p S_p(p)[W_p(p,\Delta\psi) - \overline{W}_p(p,\Delta\psi)]\,\mathrm{d}p\,\mathrm{d}\Delta\psi$$

which, when converted to a histogram, is

$$[N_+(\Delta\psi_i \to \Delta\psi_j) - N_-(\Delta\psi_i \to \Delta\psi_j)] = \int_0^\infty \int_{\Delta\psi_i}^{\Delta\psi_j} K_p S_p(p)[W_p(p,\Delta\psi) - \overline{W}_p(p,\Delta\psi)]\,\mathrm{d}p\,\mathrm{d}\Delta\psi = \int_0^\infty K_p S_p(p)\,\mathrm{d}p \left(\int_{\Delta\psi_i}^{\Delta\psi_j} W_p(p,\Delta\psi)\,\mathrm{d}\Delta\psi - \int_{\Delta\psi_i}^{\Delta\psi_j} \overline{W}_p(p,\Delta\psi)\,\mathrm{d}\Delta\psi \right).$$

This can be solved for $S(p)\,\mathrm{d}p$.

Then, substitution for $S(p)\,\mathrm{d}p$ in either N_+ or N_- gives $S_\pi(p)\,\mathrm{d}p$ with the intensities normalized to one another, but not absolutely.

Appendix 2. The weighting factors

The functions

$$\int_{\Delta\psi_i}^{\Delta\psi_j} W_k(p, \Delta\psi)\, \mathrm{d}\Delta\psi \qquad \text{and} \qquad \int_{\Delta\psi_i}^{\Delta\psi_j} \overline{W}_k(p, \Delta\psi)\, \mathrm{d}\Delta\psi$$

must be evaluated for protons and pions in order to derive the momentum spectra.

They are given by

$$W_k(p, \Delta\psi)\, \mathrm{d}\Delta\psi = \int_{\psi_0}\int_{\phi_0} A(\psi_0, \Delta\psi) B_k(\psi_0) C_k(\phi_0) D(\phi_0) P_k(p, \psi_0, \phi_0, \Delta\psi)\, \mathrm{d}\psi_0\, \mathrm{d}\phi_0 \qquad (A.1)$$

where $\int_{\Delta\psi_i}^{\Delta\psi_j} W_k(p, \Delta\psi)\, \mathrm{d}\Delta\psi$ and $\int_{\Delta\psi_i}^{\Delta\psi_j} \overline{W}_k(p, \Delta\psi)\, \mathrm{d}\Delta\psi$ are given by integrating from $\Delta\psi_i = \pm|\Delta\psi_i|$ to $\Delta\psi_j = \pm|\Delta\psi_j|$ and $\Delta\psi_i = \mp|\Delta\psi_i|$ to $\Delta\psi_j = \mp|\Delta\psi_j|$ respectively.

$A(\psi_0, \Delta\psi)$ is the probability that a particle incident at a projected angle ψ_0 will be deflected through $\Delta\psi$ and accepted assuming the neutron monitor to be uniform and neglecting the gap in the X2 flash tube tray.

$B_k(\psi_0)$ is the distribution in ψ_0 for the particle type k.

ϕ_0 is the angle of incidence in a plane perpendicular to the measuring plane of the spectrograph and $C_k(\phi_0)$ is the distribution of ϕ_0 for particle type k.

$D(\phi_0)$ is the probability of a particle incident at ϕ_0 being accepted.

$P_k(p, \psi_0, \phi_0, \Delta\psi)$ is the probability that a particle of type k and momentum p incident at angles ψ_0, ϕ_0 will be deflected through an angle $\Delta\psi$.

Equation (A.1) was evaluated numerically and then integrated over the appropriate values of $\Delta\psi$ to give the required histograms.

References

Albrow M G *et al* 1972 *Nucl. Phys.* B **37** 594–620

Allkofer O C, Carstenson K and Dau W D 1971 *Proc. 12th Int. Conf. on Cosmic Rays, Hobart* vol 4 (Hobart: University of Tasmania) pp 1314–8

Antipov Yu M *et al* 1971 *Phys. Lett.* **34B** 164–6

Brooke G and Wolfendale A W 1964 *Proc. Phys. Soc.* **83** 843–52

Brooke G, Meyer M A and Wolfendale A W 1964 *Proc. Phys. Soc.* **83** 871–7

Bull R M, Coates D W, Nash W F and Rastin B C 1962 *Nuovo Cim., Suppl.* 1 **23** 28–38

Cocconi G, Cocconi-Tongiorgi K and Widgoff M 1950 *Phys. Rev.* **79** 768–80

Conversi M and Gozzini A 1955 *Nuovo Cim.* **2** 189–91

Earnshaw J C, Orford K J, Rochester G D, Somogyi A J, Turver K E and Walton A B 1967 *Proc. Phys. Soc.* **90** 91–108

Gardener M, Kisdnaswamy S, Rössle E and Wolfendale A W 1957 *Proc. Phys. Soc.* **70** 687–99

Giacomelli G 1970 *Progress in Nuclear Physics* vol 12 (Oxford: Pergamon) pp 77–163

Griffiths W K, Harman C V, Hatton J and Ryder P 1966 *Proc. 9th Int. Conf. on Cosmic Rays, London* vol 1 (London: The Institute of Physics and The Physical Society) pp 475–7

Hatton C J 1971 *Progress in Elementary Particle and Cosmic Ray Physics* vol 10 (Amsterdam: North-Holland) pp 1–100

Hatton C J and Tomlinson E V 1968 *Nuovo Cim.* B **53** 63–72

Hayman P J and Wolfendale A W 1962 *Proc. Phys. Soc.* **80** 710–28

Hook J R and Turver K E 1974 *J. Phys.* A: *Math., Nucl. Gen.* **7** 765–78

Joseph P M 1969 *Nucl. Instrum. Meth.* **75** 13–17

O'Connor P V and Wolfendale A W 1960 *Nuovo Cim., Suppl.* 2 **15** 202–10

Orford K J 1968 *PhD Thesis* University of Durham

Rossi B 1948 *Rev. mod. Phys.* **20** 537–83

Shen Ming-Liang 1968 *Nuovo Cim., Suppl.* 4 **6** 1177–224

Simpson J A 1957 *Ann. IGY* (London: Pergamon Press) part 7

Subrahmanian A 1962 *PhD Thesis* University of Madras